JOURNAL OF THERMOPHYSICS AND HEAT TRANSFER
Vol. 22, No. 2, April–June 2008

Heat Transfer Within Carbon Nanotubes During Electron Field Emission

Jaime A. Sanchez,* M. Pinar Mengüç,† and King-Fu Hii‡
University of Kentucky, Lexington, Kentucky 40506-0108
and
R. Ryan Vallance§
The George Washington University, Washington, D.C. 20052

DOI: 10.2514/1.34165

In this paper, we present a methodology to simulate heat transfer within an isolated carbon nanotube attached to an etched tungsten tip during field emission of an electron beam. The simulations predict the field enhancement, emission current, temperature of the carbon nanotube, and distribution of electrons arriving on a target surface. The method integrates electrostatic and transient thermal finite element analyses with algorithms for modeling the field emission (based on Fowler–Nordheim approximation), heating/cooling due to emitting energetic electrons (Nottingham effect), and computation of electron trajectories. Results are presented for the axisymmetric case of an open-ended carbon nanotube separated by a 13.43-μm-gap distance from a flat surface, with voltages ranging between 65 and 145 V. Results suggest that heating of the carbon nanotube is due to the combined Nottingham effect and Joule heating when the current is below about 0.1 pA and that it is solely due to Joule heating for higher currents. Comparisons with the experimental data show very good agreement for the case studied.

Nomenclature

A_c = area of cross section
C_P = specific heat
d = exponential function
e = electron charge
F = electric field
F_{ij} = shape view factor
h_r = radiative coefficient
I = total field emission current
k = thermal conductivity
k_B = Boltzmann constant
J = field emission current density
J_i = radiosity at node i
J_0 = field emission current density at 0 K
L = length
m = constant
m_e = electron mass
P = perimeter
p = dimensionless constant
Q''' = Joule heating
q_N = Nottingham effect
q_W = heat flux dissipated toward tungsten
R = electrical resistance
$\boldsymbol{r}_i$ = vector position of electron i
$\boldsymbol{r}_{ij}$ = vector distance between electron i and j
T = temperature
T_I = inversion temperature
$t(y)$ = elliptical function
V = applied voltage
$\forall$ = volume
$v(y)$ = elliptical function
y = elliptical function
ε = emissivity
ε_r = relative permittivity
ε_0 = permittivity of the vacuum
λ = field amplification factor
ρ = material density
ρ_e = charge density
ρ_{elec} = electrical resistivity
σ = Stephan–Boltzmann constant
Φ = electron work function

Received 20 August 2007; revision received 30 November 2007; accepted for publication 2 December 2007.

*Ph.D. Candidate, Department of Mechanical Engineering, 318 Ralph G. Anderson Building. jasanc0@engr.uky.edu.
†Professor, Department of Mechanical Engineering, 269 Ralph G. Anderson Building. menguc@engr.uky.edu.
‡Ph.D. Candidate, Department of Mechanical Engineering, 015 Ralph G. Anderson Building.
§Assistant Professor, Department of Mechanical and Aerospace Engineering, 738 Academic Center.

I. Introduction

FIELD emission devices have been demonstrated and contemplated for a wide range of electronic applications, including flat-panel displays, power diodes, transistors, and electron microscopy [1,2]. Recently, Vallance et al. [3] proposed the concept for nanoscale machining based on field emission of electrons from a carbon nanotube (CNT) attached to a tungsten filament (cathode). Initial heating of a workpiece (anode) located axially a small distance from the cathode is done with a laser beam to produce threshold heating of the entire anode. Electrons emitted from the cathode, via field emission, transfer their kinetic energy to produce heating and material removal in a nanoscale region on the surface of the anode.

The plausibility of this concept has been explored theoretically in other studies, and experimental work has begun. Wong et al. [4] analyzed the effect of the electrons inside the workpiece by combining the Monte Carlo method solution of the electron transport equation with the two-temperature model to analyze the transient temperature profiles within the workpiece when a focused high-energy electron beam impinged on its surface. Hii et al. [5] conducted experiments to study the field emission characteristics of the CNT. These studies showed that the concept may work for gold and other materials if a minimum accelerating voltage can be applied. They also show that the shape of the CNT's tip may significantly affect the field emission profile, which in turn alters the electron distribution within a workpiece.

Noting that energized electrons within the workpiece are the main contribution to the concept of nanomachining, it is important to

further investigate this problem, which requires a multiphysics approach. Sanchez et al. [6] studied the effect of the tip's geometry on the distribution of the deposited electrons within the workpiece. This paper continues the theoretical investigation of this concept by concentrating on the multiphysics phenomena within the tungsten filament, CNT, and electron beam. A method for using finite element analyses to simulate heating within the isolated CNT and tungsten filament is presented. The simulations also predict the field enhancement at the CNT tip, the emission current, and the spatial distribution of the electrons arriving on the workpiece. The method integrates electrostatic and transient thermal finite element analyses with algorithms for modeling the field emission, heating/cooling due to emitting energetic electrons (Nottingham effect), and the computation of electron trajectories.

II. Multiphysics Model

Three physical phenomena occur during field emission. The first is the process of electron field emission, in which quantum tunneling of electrons occurs from the tip of the CNT [7]. The second phenomenon is the motion of the electrons as they accelerate toward the anode due to the presence of the electric field [6]. These electrons are deposited on the anode with a spatial distribution determined by their individual trajectories as obtained by integrating Newton's equations for a particle in motion. The third phenomenon is the heat conduction through the probe due to the emission of electrons and the radiation from the hot probe toward the surrounding vacuum and the anode. These phenomena are coupled and cannot be analyzed independently.

A. Field Emission in a Static Electric Field

Field emission of electrons from a surface involves quantum tunneling through a potential barrier into vacuum. Fowler and Nordheim [7] described the physics of field emission from a planar metallic surface in their classic paper. Later, it was found that long and slender emitters can substantially enhance emission by increasing the local electric field near the tip of the emitter [8]. This process has been well documented in the past [9–14]. With the use of the Wentzel–Kramers–Brillouin (WKB) approximation for the transmission coefficient [14] and neglecting band-structure effects, the tunneling probability can be integrated over all energies around the Fermi energy to give the current density J as a function of the electric field F and temperature T [14]. Equation (1) expresses $J(F, T)$ in terms of the total current density J_0 and a dimensionless parameter p that measures the additional number of electrons emitted above the Fermi level as a result of the temperature [9]:

$$J(F,T) = J_0 \frac{\pi p}{\sin \pi p} \tag{1}$$

The total current density J_0 at 0 K is given in Eq. (2) [7]. It depends upon the field F, work function Φ, and two functions, $t(y)$ and $v(y)$. These functions, given in Eqs. (4) and (5), are slow-varying functions of the field F and work function Φ expressed in Eq. (3) [11].

$$J_0 = \frac{1.54 \times 10^{-6} F^2}{\Phi t^2(y)} \exp\left[-\frac{6.83 \times 10^7 \Phi^{3/2}}{F} v(y)\right] \tag{2}$$

$$y = 3.7947 \times 10^{-4} \frac{F^{1/2}}{\Phi} \tag{3}$$

$$v(y) = 1 - 1.0125 y^{1.71} \tag{4}$$

$$t(y) = 1 + 0.1156 y^{1.4} \tag{5}$$

An expression for the dimensionless parameter p is given in Eq. (6), and it depends on the temperature T and the parameter d. A Taylor series expansion of the tunneling probability in the WKB approximation [14] yields the expression for d, given in Eq. (7).

$$p = \frac{k_B T}{d} \tag{6}$$

$$d = 9.76 \times 10^{-9} \frac{F}{t(y)\Phi^{1.5}} \tag{7}$$

In Eqs. (1–7) the units are J, J_0 (A/m^2), F (V/m), Φ, d (eV), and T (K), and k_B (8.62×10^{-5} eV/K) is Boltzmann's constant. Equation (1) breaks down at high temperatures when $p \geq 1$ and it becomes unreliable when p exceeds about 0.7 [9]. For field strengths considered in this paper, which are typically below 8 V/nm, this corresponds to temperatures on the order of 1600°C. Results presented later suggest that the temperature of the CNT can reach this range, and so this limit on Eq. (1) provides an upper bound in the validity of these simulations. In this paper, we estimate an effective value of p by calculating the total emission current as a function of temperature, integrating Eq. (1), and comparing it with the emission current obtained by integrating Eq. (2). The results are shown later. Paulini et al. [15] studied the validity of Eq. (1) for a range of work functions and applied electric fields. They found that it deviates from the actual current density when $\Phi < 3.5$ eV and $F > 9$ V/nm. This limit is not of concern to the present work, because we are operating at lower fields, and the work function of a CNT is typically ~4.7 eV.¶

As discussed by Hii et al. [5], one of the key parameters to understanding the emission current is the area of which electrons are emitted from the tip of the CNT. In their experimental work, they estimated an effective emission area A_{eff} by fitting Eq. (1) to experimentally measured $I(V)$ data. In this paper, the emission area is determined by considering the variation of the electric field over the surface of the CNT. A field strength of about 3 V/nm is commonly assumed to be the threshold for initiating field emission in CNTs [9]. Therefore, an estimate of the emission area A_e is provided by the surface area over which the field exceeds 3 V/nm.

To determine the field strength, which is necessary for evaluating Eq. (1), we begin the simulations with an electrostatic finite element analysis. The field in the gap between the cathode (CNT and tungsten tip) and anode (workpiece) is computed by solving Eq. (8):

$$\nabla \varepsilon_r \varepsilon_0 (\nabla V) = \rho_e \tag{8}$$

where ε_r is the relative permittivity of the medium, ε_0 (8.8419×10^{-12} C^2/Nm^2) is the permittivity of the vacuum, and ρ_e is the charge density of the medium. Equation (8) can be simplified when the medium is a vacuum ($\varepsilon_r = 1$) with zero charge density so that $\rho = 0$. Then the problem reduces to solving

$$\nabla^2 V = 0 \tag{9}$$

with $\nabla^2 V = \nabla F$, where F is the electric field. The boundary conditions for the solution of Eq. (9) are established by setting the surface of the CNT and tungsten tip to ground potential (0 V) and setting the workpiece anode surface to a bias voltage of V_e. In our studies, V_e ranges between 65 and 145 V. Boundaries far away from the probe and the workpiece are considered to be electrically insulated to account for the vacuum.

B. Electron Trajectories

The trajectories of emitted electrons are governed by Newton's equations of motion:

$$\frac{\mathrm{d}^2}{\mathrm{d}t^2} \boldsymbol{r}_i = \frac{e\boldsymbol{F}}{m_e} + \frac{1}{4\pi\varepsilon_0 m_e} \sum_i \sum_{i \neq j} \frac{e^2}{|\boldsymbol{r}_{ij}|^2} \tag{10}$$

where $\boldsymbol{r}_i$ is the position of electron i, $\boldsymbol{r}_{ij}$ is the distance between two

¶See Sec. II.D for a complete list of all thermophysical properties considered in this paper.

neighboring electrons, $\boldsymbol{F}$ is the applied electric field, and e (1.602×10^{-19} C) and m_e (9.31×10^{-31} kg) are the electron charge and mass. The first term on the right-hand side of Eq. (10) corresponds to the electrostatic force applied on a traveling electron due to the presence of the electric field; the second term on the right-hand side corresponds to the Coulomb repulsion forces between moving electrons. Because the value of the electric field can be determined from Eq. (9), the preceding equation can be evaluated to give the electron trajectory from the probe toward the workpiece.

The positions that the electrons strike on the workpiece are used to map the current density distribution, calculated with Eq. (1), on the surface. Sanchez et al. [6] studied the effect of the CNT's shape on deposition profiles of the emitted electrons. We follow that methodology in this work. The current density distribution on the surface of the workpiece is used as a heat flux term within the heat transfer calculations.

C. Heat Transfer Models

In 1936, Nottingham [16] discovered that a heat flux is present during field emission from tungsten filaments. Considering that the presence of the field emission current should cause heating of the cathode, it was found that the temperature attained by the field emitter was, in some instances, less or more than that predicted by traditional calculations. Charbonnier et al. [17] found that there is a stabilizing factor provided by the energy exchange resulting from the difference between the average energy of the emitted electrons E and that of the replacement electrons E' during the process. In general, E' is taken as the Fermi energy E_f. Energy levels above E_f are empty, and in pure-field emission at 0 K, all emitted electrons have less than the Fermi energy, and the Nottingham effect produces heating of the cathode. However, if the cathode temperature is increased (thermofield emission), energy levels above E_F become populated and contribute preferentially to the emission, causing a decrease in the average heat transfer per emitted electron. If the temperature of the emitter exceeds an "inversion" temperature T_I, E becomes greater that E_F, reversing the effect and cooling the cathode. The inversion temperature can be quantified with [17]

$$T_I = 5.67 \times 10^{-5} \frac{F}{\Phi^{1/2} t(y)} \tag{11}$$

This Nottingham effect therefore provides a heat flux q''_N, given in Eq. (12), that acts on the surface region in which the field emission occurs. It can be quantified with [18]

$$q''_N = \frac{J\varepsilon}{e} \tag{12}$$

where J is the current density given in Eq. (1), $\varepsilon = -\pi p d \cot(\pi p)$, and e is the electron charge. If the temperature of the cathode T is such that $T < T_I$, then the sign of the heat flux is positive and thus the Nottingham effect acts a heating mechanism. It will be a cooling effect when $T > T_I$.

The flow of current through the cathode also causes the temperature to rise due to Joule heating and it was discussed by different groups. Swanson et al. [14] considered both the Nottingham effect and Joule heating in determining the temperature variation produced by the energy-exchange processes accompanying field-electron emission. In the case of the Nottingham effect, the energy exchange between the conduction electrons and the lattice is expected to occur within a fraction of an emitter-tip diameter (approximately 100 nm) because of the extremely short mean free path of conduction electrons near the Fermi energy with respect to electron–phonon and electron–electron interactions.

Gratzke and Simon [18], on the other hand, found that the Joule heating due to field-emitted electrons produces a negligible effect. They considered the emitter as a thin rod of gold of length l that was heated by a current density j, with boundary conditions $\partial T/\partial x = 0$ at $x = 0$ and 1. They found that the temperature increase of the emitter due to Joule heating alone was almost negligible and they concluded that the Nottingham effect was responsible for heating the emitter.

The heat transfer in the cathode is modeled using the transient heat conduction equation with volumetric heat generation:

$$\rho C_p \frac{\partial T}{\partial t} = \nabla(-k\nabla T) + Q''' \tag{13}$$

where k is the thermal conductivity, ρ is the density, C_p is the specific heat, T is the temperature, and Q''' is the volumetric heat generation term due to Joule heating. It is defined as

$$Q''' = \frac{I^2 R}{\forall} \tag{14}$$

where I is the total emission current from integrating Eq. (1), R is the resistance, and $\forall$ is the volume of the probe.

Equation (13) is subject to conduction and radiation boundary conditions. Because we model only a section of the tungsten filament, the heat conducted to the remainder part is modeled using Eq. (15):

$$q_W = \sqrt{h_r P k A_c} \frac{\cosh mL}{\sinh mL} (T - T_\infty) \tag{15}$$

where $h_r = \varepsilon\sigma(T + T_\infty)(T^2 + T_\infty^2)$ is the equivalent radiative coefficient [19], A_c is the cross-sectional area of the cylinder, and $m^2 = h_r P/kA_c$.

We consider the radiation heat transfer from the cathode, although the rigorous calculations of near-field radiation effects are not performed. It is known that when the distance between two hot bodies is smaller than the wavelength of the thermal radiation, there exists radiation enhancement by tunneling of evanescent waves [20]. The critical separation between the two bodies can be estimated from Wien's displacement law as $\lambda_T T = 2898.8\ \mu\text{m K}$. Recently, Francoeur and Mengüç [21] have reported that the critical distance is actually 3 times larger than that predicted by Wien's law. This means that for a surface temperature $T = 293$ K, the critical gap distance to be considered is $\lambda_T \sim 30\ \mu$m, which suggests that the near-field effects may play a role in heat transfer calculations. However, the mathematical formulation to study near-field effects in radiative transfer is very cumbersome even for the relatively simpler case of two parallel plates [21], let alone for cylindrical geometries. In this paper, we first use the radiosity node method to estimate the radiation exchange [19]:

$$\frac{E_{bi} - J_i}{(1 - \varepsilon_i)/\varepsilon_i A_i} = \sum_{j=1}^{N} \frac{J_i - J_j}{(A_i F_{ij})^{-1}} \tag{16}$$

where E_{bi} is the irradiation, A_i is the total area, ε_i is the emissivity of surface i, F_{ij} is the shape factor between surfaces i and j, J_k is the radiosity from surface k, and N is the total number of surfaces. The formulation in Eq. (16) neglects any effects attributed to near-field radiation. To estimate the error in our calculations, the total radiative heat flux derived from Eq. (16) is multiplied by a factor of 1000. This is done to study any potential variations in the resulting temperature profile on the cathode that may arise from an enhanced radiative effect. This is discussed further in Sec. III.

D. Thermophysical Properties

Table 1 shows the properties used for tungsten [19,23,25,29] and the CNT [22,24,26–28,30–34] as reported in the literature. The thermophysical properties used for the CNT and shown in Table 1 fall in the range of the most probable values reported for multiwalled CNTs [22,24,26–28,30].

Finding adequate properties for the CNT is not as straightforward as for tungsten. Several authors have investigated the thermophysical properties of single-wall [32–35] and multiwall [22,27,31] CNTs, with a wide range of variation of the properties depending on the experimental conditions. The effect of these variations on the heat transfer calculations has been explored recently by Sanchez and Mengüç [36].

Table 1 Thermophysical properties

Property	Tungsten, W	CNT
Density ρ, kg/m^3	19,250 [19]	1330 [22]
Emissivity ε	$-0.0434 + 1.8624E - 4T - 1.954E - 8T^2$ [23]	1 [24]
Resistivity ρ_{elec}, Ωm	$48\text{E} - 9(1 + 4.8297\text{E} - 3(T - 273) + 1.663\text{E} - 6(T - 273)^2)$ [25]	$1.7\text{E} - 6$ [26]
Specific heat C_p, J/kg K	$4\text{E} - 14T^5 - 3\text{E} - 10T^4 + 7\text{E} - 07T^3 - 0.0008T^2 + 0.4501T + 53.299$ [19]	$0.0004T^2 + 1.4429T - 10.238$ [27]
Conductivity k, W/mK	$1\text{E} - 11T^4 - 8\text{E} - 08T^3 + 0.0002T^2 - 0.2568T + 230.88$ [19]	3000 [28]
Work function, eV	4.8 [29]	4.7 [30]

E. Finite Element Analysis

We model a multiwalled CNT synthesized by chemical vapor deposition attached to an etched tungsten filament. The tungsten filament was prepared by electrochemical etching in 2.0N NaOH standardized solution with dc voltages. Figure 1 shows a scanning electron microscope (SEM) image of the ensemble.

As seen in Fig. 1 the CNT is attached to the side of the etched tungsten filament's tip. From a simulations point of view, this creates an antisymmetric model that requires 3D analysis of the geometries. However, the tilt angle of the CNT with respect to the tungsten filament is approximately 0.15 deg. In this study, we assume the CNT is placed directly on top of the tip of the tungsten filament, allowing for a 2D axisymmetric model, shown in Fig. 2a.

In Fig. 2b, we show the way the CNT is attached to the tungsten filament. The section shown of the CNT corresponds to a cut of the wall, assumed to be 1.6 nm thick.

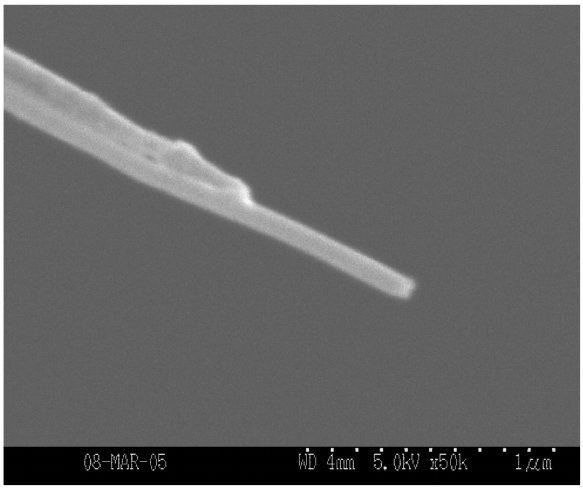

Fig. 1 SEM image of the CNT attached to an etched tungsten probe. The CNT has dimensions of ~60 nm in diameter and 2.1 μm in length. The protruding length is ~600 nm and the estimated wall thickness is 1.7 nm.

We optimize the number of elements used in COMSOL Multiphysics 3.2b in the following way: we calculate the electric field from Eq. (9) for a given number of elements, then Eq. (2) is used to calculate the current density as a function of the electric field. Finally, we integrate the current density on the periphery of the CNT to calculate the total emission current. We tested four cases with an increasing number of elements and found that using 151,836 elements gives the best accuracy when we compare our integrated current density with the experiments of Hii et al. [5]. The discretized mesh used in our simulations is shown in Fig. 3.

The key feature of the mesh shown in Fig. 3 is that more elements are used on the tip of the CNT to avoid singularities in the finite element solution due to the small wall thickness. For the heat transfer calculations, we used the same mesh. The solution methodology followed for the finite element method is outlined in Fig. 4.

The simulations are run on a Windows XP machine, Pentium 4, 3.2 GHz and 4 Gb of RAM. For each applied voltage considered, the elapsed time to determine the electric field distribution is approximately 8 s. However, the electron trajectories require a larger time because the integration of the equations of motion is done for various electrons at the same time. An average time of 3 h is required to determine the trajectories for each applied voltage. The heat transfer calculations required approximately 30 s for each applied voltage.

III. Results and Discussion

A. Electrostatic Calculations

The electric field distribution on the CNT's tip and the current density determined using Eq. (2) are shown for a gap distance of 13.43 μm for three applied voltages.

We studied a range of input voltages from 65 to 145 V. In Fig. 5, only three applied voltages are shown for clarity. The curves in Fig. 6 do not correspond to constant electric field (Fig. 5a) or constant current density (Fig. 5b). They represent the variation of those quantities on the surface of the CNT as a function of applied voltage. The dashed line shown in both figures can be rotated and centered on the middle of the wall of the CNT to give the values of the electric field and current density (Figs. 5a and 5b, respectively). The main trend is that when the voltage increases, so does the electric field on

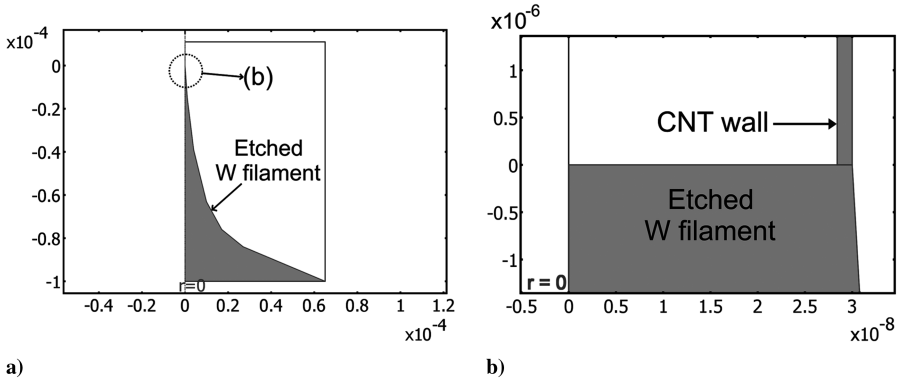

Fig. 2 Computational model used: a) geometry of the CNT attached to the tungsten filament and b) attachment point. The model is axisymmetric with the revolving axis depicted as $r = 0$. Only the etched part of the tungsten filament is shown; the total length of the tungsten filament is 1 in. The dimensions are in meters. Note that Fig. 2b is enlarged from Fig. 2a as indicated, and the coordinate axes coincide.

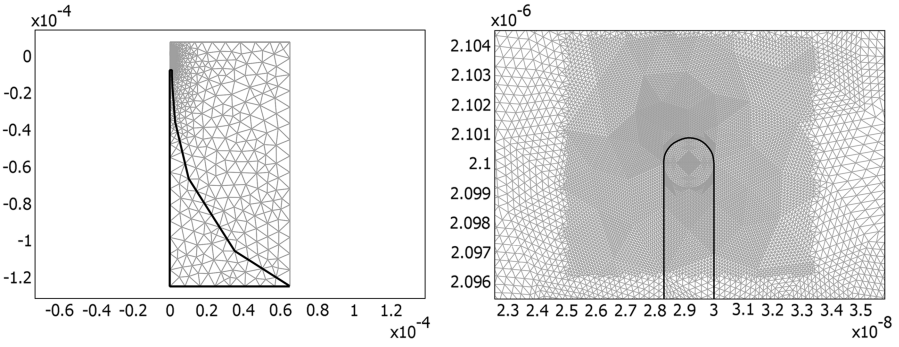

a) b)

Fig. 3 Finite element model: a) mesh used to solve the problem and b) close-up of the adaptive mesh used at the tip of the CNT. The dimensions are in meters. Note that Fig. 2b is enlarged from Fig. 2a as indicated, and the coordinate axes coincide.

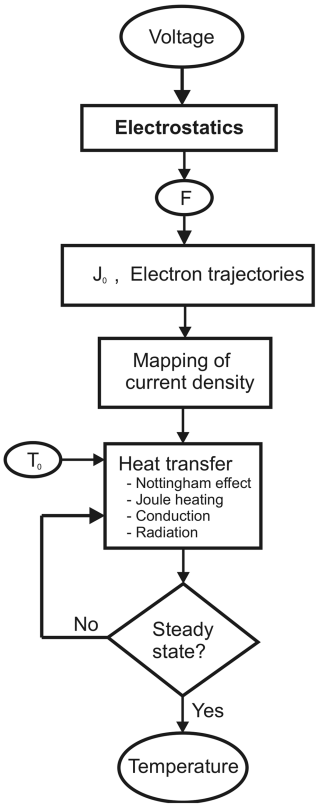

Fig. 4 Solution methodology of the finite element problem.

the tip. It is noticeable that the maximum electric field for a given voltage is not on the apex of the CNT wall, but rather located in positions outside of the CNT. Also, the electric field exhibits a variation of approximately 50% between its maximum and minimum values found closer to the sides of the wall. This is because the apex of the wall creates a large enhancement of the electric field. We calculated the field amplification factor defined as $\lambda = dF/V$, where V is the applied voltage, d is the gap distance, and F is the electric field. We found that the field enhancement factor is not sensitive to the applied voltage and its maximum value of 671.5 correlates well with the experimental data of Hii et al. [5] for a gap distance of 13.43 μm. The current density in Fig. 5b shows even larger variations. We plotted the log of the current density because of differences in the order of magnitude between applied voltages. Comparing Figs. 5a and 5b, it can be seen that the variations in the electric field of approximately 50% on the wall produce large variations in the current density. These small values of current density are observed specially in the lower parts of the apex of the wall.

One of the key parameters in estimating the total emission current from the CNT is the knowledge of the emitting area [5]. In our simulations, the total emission current can be determined by integrating the current density on the surface of the CNT, assuming that emission occurs for every point in the surface. Because the current density shows large variations, there are parts of the wall surface that make negligible contributions to the current. Therefore, considering the entire wall surface in the integration should provide a minimum error in the calculation. As the voltage increases, however, it is possible that larger areas on the surface become active electron emission sites and an increase in the emitting area is expected. This effect is shown in Fig. 6a.

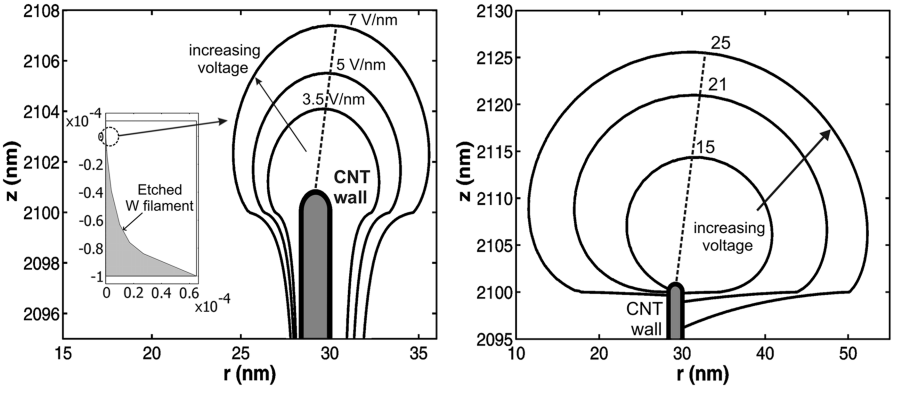

a) b)

Fig. 5 Electrostatic results: a) electric field distribution on the CNT's tip (inset is in meters) and b) log of the current density on the CNT's tip. The gap distance is 13.43 μm and the plots correspond to 70, 100, and 140 V. Both figures are enlarged from the inset on the left. The axis of symmetry is at $r = 0$. The dashed line can be used for reference as the values indicated for each intersection correspond to the magnitudes of the normal electric field or current density at that point. The dashed line can be rotated on the center of the wall of the CNT to give the values of the electric field or current density at the intersection points. The values shown correspond to the values of the electric field and current density at that particular intersection.

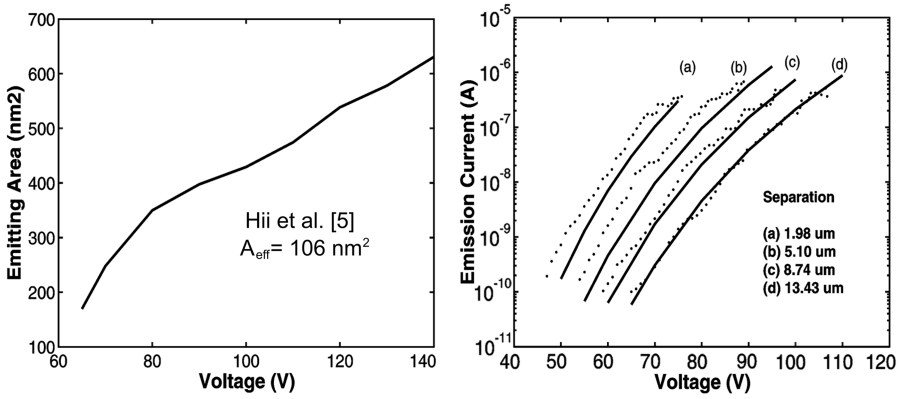

a) b)

Fig. 6 Electrostatic results: a) emitting area as a function of the applied voltage for a separation distance of 13.43 μm and b) emission current vs voltage. The points correspond to the experimental data by Hii et al. [5].

The emitting area is estimated by calculating the area on the CNT surface for which the local values of the field strength F exceed 3 V/nm. We found that this criterion also gives the surface area for which 99.9% of the total emission current is obtained when integrating Eq. (1). Only the case with a separation distance of 13.43 μm was considered; however, a similar trend is expected for other cases. We found that as the applied voltage increases, so does the emitting area, in an almost linear fashion. As the voltage increases, the field strength on the surface of the CNT also increases, creating new sites for electron emission. This increasing area is in contrast with the findings of Hii et al. [5]. In their work, an effective emitting area was calculated to fit the Fowler–Nordheim theory [Eq. (2)] that was assumed constant with the separation distance and the applied voltage.

The field emission experiments of Hii et al. [5] began with the detection of the cathode via measurements of the emission current when the separation distance is slowly closed until a small bias voltage produced a sudden current increase under a vacuum base pressure of about 4×10^{-8} mbar (3×10^{-8} torr). Once the surface was detected, the voltage was increased to obtain the $I(V)$ curve for that separation distance. The first separation distance considered was 13.43 μm. The voltage was increased up to a certain point and the 24 measurements of current were made (Fig. 6b). Then the separation distance was decreased and the experiment was repeated. We found excellent agreement between our predicted emission current and their measured values, particularly for the largest separation distance. For this case, we simulated a CNT with 60 nm in diameter, 2.1 μm in length, and a wall thickness of 1.6 nm (Fig. 1). However, our calculations predict a current much lower than what was measured. This could be attributed by changes in the morphology of the tip due to the process of field emission. It has been reported that during field emission the outer carbon rings of the CNT can become detached [37]. This would cause a sudden increase in the sharpness of the tip and thus create additional field enhancement.

We also determined the electron trajectories from the tip of the cathode toward the anode following the procedure of Sanchez et al. [6]. Each point on the tip of the cathode is assumed to be a possible electron emission site. From there, we calculate the trajectories of the emitted electrons via integrating Eq. (10). The final position of the emitted electrons on the surface of the anode can then be used to map the current density on the surface. The electron trajectories and the mapped current density on the workpiece are shown in Fig. 7 for a gap distance of 13.43 μm (Figs. 7a and 7b, respectively).

In Fig. 7a we plotted the initial position of an electron on a CNT's tip (abscissa) with its final position on the workpiece (ordinate). For a given separation distance, the electron spread on the workpiece is not sensitive to increases in voltage [6]. We found that the maximum electron spread is approximately 3 times the gap distance for this particular CNT geometry. Using the methodology outlined by Sanchez et al. [6], we map the current density on the workpiece using the final positions of the electrons. The pattern that results on the surface corresponds to a ring with the highest current density at approximately 500 nm away from the center of the CNT. Ringlike patterns due to emission from a CNT have been reported in the past [38] and result from a large radial component of the electric field near the flat tip of an open-ended CNT. This gives the electrons a large radial velocity component that gives a large spread of the emitted electron beam.

The results presented in this section are used in the heat transfer calculations. Because the closest match between experiment and

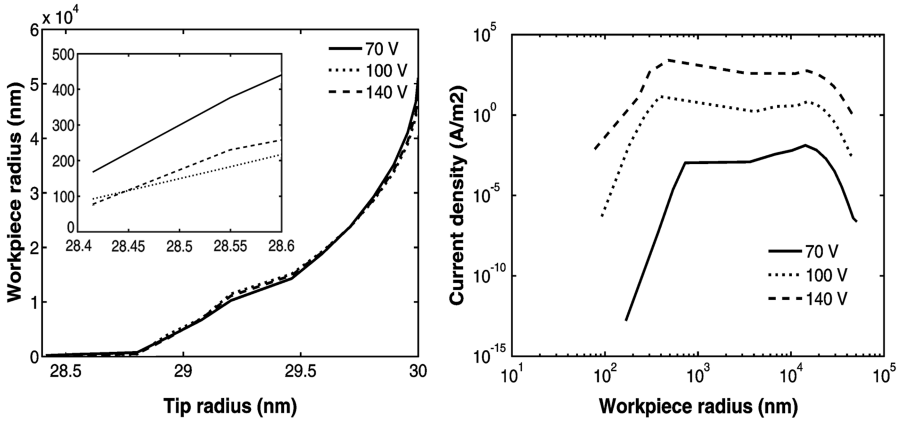

a) b)

Fig. 7 Results of electron trajectories: a) electrons that are emitted from a radial location on the tip (abscissa) impact at a radial location on the workpiece (ordinate) (the inset has the same dimensions, but shows the results for the smaller radii in more detail) and b) current density on the workpiece mapped following [6]. The axis of symmetry is at $r = 0$. The separation distance is 13.43 μm.

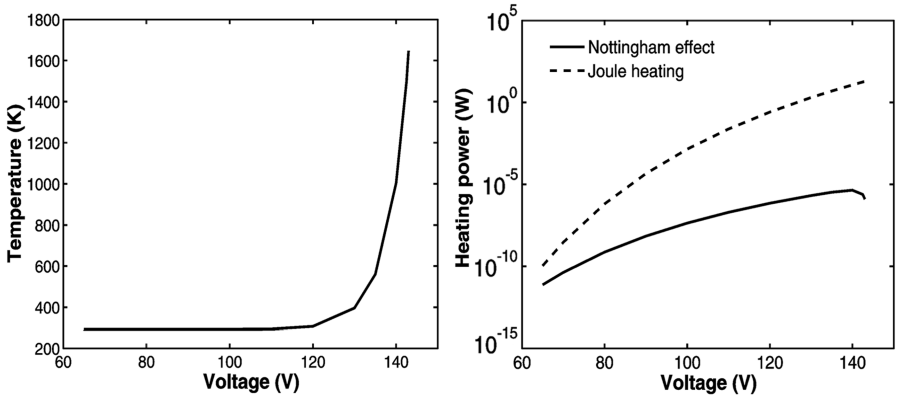

Fig. 8 Heat transfer result: a) maximum temperature vs applied voltage and b) comparison between the Nottingham effect and the Joule heating.

simulation was found with a separation distance of 13.43 μm, the results presented next are based only on that case.

B. Heat Transfer Calculations

With the results of the previous sections, we solve Eq. (13) to find the temperature evolution of the CNT as a function of the applied voltage. In Fig. 8, the maximum temperature on the CNT is shown as a function of the applied voltage for a separation distance of 13.43 μm (Fig. 8a), as well as the main sources of heating of the CNT during the process (Fig. 8b). The time required to reach a steady-state solution of Eq. (13) was approximately 0.01 ms.

The temperature increase of the CNT is almost negligible up to approximately 120 V, as seen in Fig. 8a. When the voltage is increased, the temperature rises steeply, almost exponentially. Given that the melting point of a multiwalled CNT can be considered as that of carbon (3773 K), even with an exponential rise in temperature, larger currents could be obtained, providing that the substrate on which the CNT is deposited can withstand the high temperatures [24,39]. In the recent work by She et al. [39] the heat transfer during field emission from a CNT deposited on top of a silicon tip was studied. At high emission currents, it was found that the temperature of the CNT increased far beyond the melting point of the silicon tip on which it was deposited (greater than 1683 K), therefore causing a breakdown of the emitter (CNT–silicon tip). In their work, the field emission current was calculated by integrating the full current density equation studied in the work by Murphy and Good [12] that has no discontinuities for large temperatures. The mechanism responsible for this breakdown was attributed to a "thermal runaway" in which the field emission current increased uncontrollably with temperature past a certain critical electric field. As the electric field increases, the temperature rise of the CNT is steady and reaches a plateau at a certain value. Slight increases in the electric field beyond this point (less than 0.01%) cause a rapid uncontrollable rise in the temperature. Given that tungsten has a much higher melting point (3680 K), it could probably withstand the higher temperatures attained during this process. The validity of Eq. (1) breaks down when the nondimensional parameter p is greater than or equal to unity, which mathematically causes the equation to asymptote to infinity at high temperatures. Therefore, we only considered our simulations up to $p \sim 0.5$, where 0.7 is the highest recommended value [9].

The main heat sources on the CNT are the Joule heating [Eq. (14)] and the Nottingham effect [Eq. (12)]. The former is always positive because it is a function of the emission current and the resistance. The latter, however, can have negative values depending on the temperature: if it is lower than the inversion temperature T_I [Eq. (11)], then the Nottingham effect heats the emitter; if it is higher, it cools it. To determine the overall Nottingham effect, we integrated Eq. (12) on the surface of the CNT. The Joule heating was determined by integrating Eq. (14) over the volume of the probe (CNT attached to tungsten filament). Both effects are compared in Fig. 8b as a function of the applied voltage. Our calculations show that the main source of heating of the cathode is the Joule heating. For small voltages, it seems that the Nottingham effect and the Joule effect tend to be comparable. As the voltage increases, the Nottingham effect is negligible in comparison with the Joule heating. This is in contrast to the findings of Gratzke and Simon [18] in which the Joule heating was found to be negligible. In their work, the volume considered in the calculation of the Joule heating was that of the CNT only. However, in more realistic conditions, the cathode on which the CNT is located also contributes to the Joule heating because the field emission current flows through it. We are currently investigating the dependence on the cathode geometry of the magnitude of the Nottingham effect and the Joule heating [36]. There is a noticeable decrease in the Nottingham effect close to 140 V, indicating the possibility that some points on the tip have a temperature above the inversion temperature. The inversion temperature is shown in Fig. 9.

The behavior of the Nottingham effect for high voltages (Fig. 8b) is explained in Fig. 9 via the magnitude of the inversion temperature. At some points on the tip of the CNT, the temperature rise exceeds the inversion temperature and the Nottingham effect switches from heating to cooling. The maximum value of the latter is approximately 18×10^9 W/m^2 and remains positive for a larger area on the tip. Points that are below a radius of 28.8 nm do not contribute significantly to the Nottingham effect, because for these points, the magnitude of the current density and electric fields are low and affect Eq. (12) in the same way. The overall Nottingham effect is of the heating of the cathode, even though the negative values on the integral decrease its magnitude when compared with the Joule heating.

Finally, in Fig. 10a, we compare the temperature-dependent field emission current [integral of Eq. (1)] with the zero-Kelvin approximation [integral of Eq. (2)] and the experimental data of Hii et al. [5] for a separation distance of 13.43 μm.

We found that the temperature-dependent emission current is almost the same as the temperature-independent emission current for

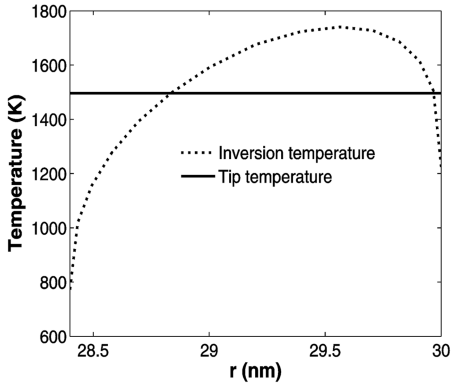

Fig. 9 Comparison between the temperature on the tip and the inversion temperature [Eq. (11)].

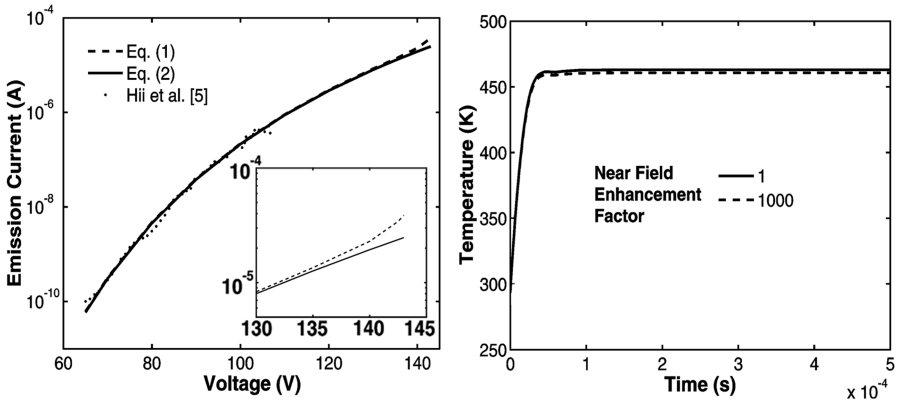

a) b)

Fig. 10 Heat transfer result: a) comparison between the total emission current from integrating Eqs. (1) and (2) with the experimental data of Hii et al. [5] (the inset has the same dimensions, but shows the results for the high voltage values in more detail) and b) near-field thermal radiation effects compared based on a constant factor. The applied voltage is 130 V.

most of the voltage range considered. This means that the effect of temperature is negligible when it comes to calculating the emission current, especially for lower voltages. Additionally, we estimate the effect of neglecting near-field thermal radiation effects on the transient temperature increase of the cathode (Fig. 10b). Two cases are considered based on an arbitrary "field enhancement factor" that multiplies the total radiative flux. In the first case, we assume that the field enhancement factor is unity (neglecting all potential near-field effects). In the second case, we use a value of 1000. For an applied voltage of 130 V, we found an error of less than 1% in neglecting all near-field thermal radiation effects. Therefore, we conclude that using the classical radiative transfer formulation is adequate for the calculations presented.

IV. Conclusions

In this paper, we investigated the thermal behavior of a CNT used as a field emitter under various applied voltages. The heat sources acting on the CNT are the Nottingham effect and Joule heating. The former is negligible with respect to the latter, except for very low voltages (less than 62 V), where the emission current is low, on the order of 0.1 pA. For higher voltages, Joule heating is the main cause of heating and as the voltage is increased it can lead to failure of the emitter. The Nottingham effect also helps to lower the temperature of the emitter for high applied voltages, because the overall temperature of the CNT rises above the inversion temperature. This behavior is very complex in nature, varying pointwisely along the surface of the CNT. Finally, we also showed that the traditional zero-Kelvin or Fowler–Nordheim approximation can be used for most of the voltage range by matching numerical calculations with experimental results. We found good agreement between our simulations of field emission and the experiments done by Hii et al. [5] for a separation distance of 13.43 μm. Therefore, the proposed methodology can be used for guiding the experiments.

Acknowledgments

This work is supported by the National Science Foundation through a Nanoscale Interdisciplinary Research Team (NIRT) award from the Nano-Manufacturing program in Design, Manufacturing, and Industrial Innovation (DMI-0210559). Additional support was received from the Kentucky Science and Education Foundation (KSEF) and the University of Kentucky. Any opinions, findings, and conclusions or recommendations expressed in this material are those of the author(s) and do not necessarily reflect the views of the National Science Foundation.

References

[1] Brodie, I., and Schwoebel, P. R., "Vacuum Microelectronic Devices," *Proceedings of the IEEE*, Vol. 82, Inst. of Electrical and Electronics Engineers, Piscataway, NJ, 1994, p. 28.

[2] Saito, Y., Nishiyami, T., Kato, T., Kondo, S., Tanaka, T., Yotani, J., and Uemura, S., "Field Emission Properties of Carbon Nanotubes and Their Application to Display Devices," *Molecular Crystals and Liquid Crystals Science and Technology, Section A: Molecular Crystals and Liquid Crystals*, Vol. 387, 2002, pp. 79–86. doi:10.1080/10587250215248

[3] Vallance, R. R., Rao, A. M., and Mengüç, M. P., "Processes for Nanomachining Using Carbon Nanotubes," U.S. Patent 6660959, Issued 9 Dec. 2003.

[4] Wong, B. T., Mengüç, M. P., and Vallance, R. R., "Nano-Scale Machining via Electron Beam and Laser Processing," *Journal of Heat Transfer*, Vol. 126, No. 4, 2004, pp. 566–576. doi:10.1115/1.1777581

[5] Hii, K. F., Vallance, R. R., Chikkamaranahalli, S. B., Menguc, M. P., and Rao, A. M., "Characterizing Field Emission from Individual Carbon Nanotubes at Small Distances," *Journal of Vacuum Science and Technology B (Microelectronics and Nanometer Structures)*, Vol. 24, No. 3, 2006, pp. 1081–1087. doi:10.1116/1.2188403

[6] Sanchez, J. A., Wong, B. T., Menguc, M. P., and Albella, P., "Field Emission and Electron Deposition Profiles as a Function of Carbon Nanotube Tip Geometries," *Journal of Applied Physics*, Vol. 101, No. 11, 2007, Paper 114313.

[7] Fowler, R. H., and Nordheim, L. W., "Electron Emission in Intense Electric Fields," *Proceedings of the Royal Society*, Vol. A119, Royal Society of London, London, 1928, p. 8.

[8] Spindt, C. A., "A Thin-Film Field-Emission Cathode," *Journal of Applied Physics*, Vol. 39, No. 7, 1968, pp. 3504–3505. doi:10.1063/1.1656810

[9] Fransen, M., "Towards High-Brightness, Monochromatic Electron Sources," Ph.D. Thesis, Technische Univ. Delft, Delft, The Netherlands, 1999.

[10] Gomer, R., *Field Emission and Field Ionization*, American Vacuum Society Classics, American Inst. of Physics, New York, 1993.

[11] Good, R. H., and Muller, E. W., *Handbuch der Physik*, edited by S. Flügge, Springer–Verlag, Berlin, 1956, p. 21.

[12] Murphy, E. L., and Good, R. H., Jr., "Thermionic Emission, Field Emission, and the Transition Region," *Physical Review B*, Vol. 102, No. 6, 1956, pp. 1464–1473. doi:10.1103/PhysRev.102.1464

[13] Stratton, R., "Energy Distributions of Field Emitted Electrons," *Physical Review. A.*, Vol. 135, No. 3A, 1964, pp. A794–A805. doi:10.1103/PhysRev.135.A794

[14] Swanson, L. W., Crouser, L. C., and Charbonnier, F. M., "Energy Exchanges Attending Field Electron Emission," *Physical Review*, Vol. 151, No. 1, 1966, pp. 327–340. doi:10.1103/PhysRev.151.327

[15] Paulini, J., Klein, T., and Simon, G., "Thermo-Field Emission and the Nottingham Effect," *Journal of Physics D: Applied Physics*, Vol. 26, No. 8, 1993, pp. 1310–1315. doi:10.1088/0022-3727/26/8/024

[16] Nottingham, W. B., "Thermionic Emission From Tungsten and Thoriated Tungsten Filaments," *Physical Review*, Vol. 49, No. 1, 1936, pp. 78–97. doi:10.1103/PhysRev.49.78

[17] Charbonnier, F. M., Strayer, R. W., Swanson, L. W., and Martin, E. E.,

"Nottingham Effect in Field and T-F Emission: Heating and Cooling Domains and Inversion Temperature," *Physical Review Letters*, Vol. 13, No. 13, 1964, pp. 397–401. doi:10.1103/PhysRevLett.13.397

[18] Gratzke, U., and Simon, G., "Mechanism of Nanostructure Formation with the Scanning Tunneling Microscope," *Physical Review. B.*, Vol. 52, No. 11, 1995, pp. 8535–8540. doi:10.1103/PhysRevB.52.8535

[19] Incropera, F. P., and DeWitt, D. P., *Heat Transfer Fundamentals*, 4th ed., Prentice–Hall, Upper Saddle River, NJ, 1996.

[20] Pendry, J. B., "Radiative Exchange of Heat Between Nanostructures," *Journal of Physics: Condensed Matter*, Vol. 11, No. 35, 1999, pp. 6621–6633. doi:10.1088/0953-8984/11/35/301

[21] Francoeur, M., and Mengüç, M. P., "Role of Fluctuational Electrodynamics in Near-Field Radiative Heat Transfer," *Journal of Quantitative Spectroscopy and Radiative Transfer*, Vol. 109, No. 2, 2008, pp. 280–293. doi:10.1016/j.jqsrt.2007.08.017

[22] Gao, G. H., Cagin, T., and Goddard, W. A., "Energetics, Structure, Mechanical and Vibrational Properties of Single-Walled Carbon Nanotubes," *Nanotechnology*, Vol. 9, 1998, pp. 184–191. doi:10.1088/0957-4484/9/3/007

[23] Forsythe, W. E., and Worthing, A. G., "The Properties of Tungsten and the Characteristics of Tungsten Lamps," *Astrophysical Journal*, Vol. 61, 1925, pp. 146–185. doi:10.1086/142880

[24] Huang, N. Y., She, J. C., Chen, J., Deng, S. Z., Xu, N. S., Bishop, H., Huq, S. E., Wang, L., Zhong, D. Y., Wang, E. G., and Chen, D. M., "Mechanism Responsible for Initiating Carbon Nanotube Vacuum Breakdown," *Physical Review Letters*, Vol. 93, No. 7, 2004, Letter 075501. doi:10.1103/PhysRevLett.93.075501

[25] Lide, D., *CRC Handbook of Chemistry and Physics*, 75th ed., CRC Press, Boca Raton, FL, 1995, p. 12.

[26] Purcell, S. T., Vincent, P., Journet, C., and Binh, V. T., "Hot Nanotubes: Stable Heating of Individual Multiwall Carbon Nanotubes to 2000 K Induced by the Field-Emission Current," *Physical Review Letters*, Vol. 88, No. 10, 2002, p. 105502. doi:10.1103/PhysRevLett.88.105502

[27] Yi, W., Lu, L., Zhang, D. L., Pan, Z. W., and Xie, S. S., "Linear Specific Heat of Carbon Nanotubes," *Physical Review B*, Vol. 59, No. 14, 1999, pp. R9015–R9018. doi:10.1103/PhysRevB.59.R9015

[28] Kim, P., Shi, L., Majumdar, A., and McEuen, P. L., "Thermal Transport Measurements of Individual Multiwalled Nanotubes," *Physical Review Letters*, Vol. 87, No. 21, 2001, Letter 215502. doi:10.1103/PhysRevLett.87.215502

[29] Muller, E. W., "Work Function of Tungsten Single Crystal Planes Measured by the Field Emission Microscope," *Journal of Applied Physics*, Vol. 26, No. 6, 1955, pp. 732–737. doi:10.1063/1.1722081

[30] Gao, R. P., Pan, Z. W., and Wang, Z. L., "Work Function at the Tips of Multiwalled Carbon Nanotubes," *Applied Physics Letters*, Vol. 78, No. 12, 2001, pp. 1757–1759. doi:10.1063/1.1356442

[31] Berber, S., Kwon, Y. K., and Tomanek, D., "Unusually High Thermal Conductivity of Carbon Nanotubes," *Physical Review Letters*, Vol. 84, No. 20, 2000, pp. 4613–4616. doi:10.1103/PhysRevLett.84.4613

[32] Fujii, M., Zhang, X., Xie, H. Q., Ago, H., Takahashi, K., Ikuta, T., Abe, H., and Shimizu, T., "Measuring the Thermal Conductivity of a Single Carbon Nanotube," *Physical Review Letters*, Vol. 95, No. 6, 2005, Letter 065502. doi:10.1103/PhysRevLett.95.065502

[33] Hone, J., Whitney, M., Piskoti, C., and Zettl, A., "Thermal Conductivity of Single-Walled Carbon Nanotubes," *Physical Review B*, Vol. 59, No. 4, 1999, pp. R2514–R2516. doi:10.1103/PhysRevB.59.R2514

[34] Hone, J., Llaguno, M. C., Biercuk, M. J., Johnson, A. T., Batlogg, B., Benes, Z., and Fischer, J. E., "Thermal Properties of Carbon Nanotubes and Nanotube-Based Materials," *Applied Physics A: Materials Science and Processing*, Vol. 74, No. 3, 2002, pp. 339–343. doi:10.1007/s003390201277

[35] Davisson, C., and Germer, L. H., "The Thermionic Work Function of Tungsten," *Philosophical Magazine*, Vol. 40, 1920, p. 746.

[36] Sanchez, J. A., and Mengüç, M. P., "Geometry Dependence on the Electro-Static and Thermal Response of a Carbon Nanotube During Field Emission," *Nanotechnology*, Vol. 19, No. 7, 2008, Paper 075702.

[37] Fujieda, T., Hidaka, K., Hayashibara, M., Kamino, T., Ose, Y., Abe, H., Shimizu, T., and Tokumoto, H., "Direct Observation of Field Emission Sites in a Single Multiwalled Carbon Nanotube by Lorenz Microscopy," *Japanese Journal of Applied Physics, Part 1: Regular Papers Short Notes and Review Papers*, Vol. 44, No. 4A, 2005, pp. 1661–1664. doi:10.1143/JJAP.44.1661

[38] Walker, D. G., Zhang, W., and Fisher, T. S., "Simulation of Field-Emitted Electron Trajectories and Transport from Carbon Nanotubes," *Journal of Vacuum Science and Technology B (Microelectronics and Nanometer Structures)*, Vol. 22, No. 3, 2004, pp. 1101–1107. doi:10.1116/1.1755214

[39] She, J. C., Xu, N. S., Deng, S. Z., Chen, J., Bishop, H., Huq, S. E., Wang, L., Zhong, D. Y., and Wang, E. G., "Vacuum Breakdown of Carbon-Nanotube Field Emitters on a Silicon Tip," *Applied Physics Letters*, Vol. 83, No. 13, 2003, pp. 2671–2673.